

Analysis of a strip footing on a homogenous soil using element free Galerkin method

Aashiq H. Ganaie^a and Vishwas A. Sawant*

Department of Civil Engineering, Indian Institute of Technology Roorkee – 247667, India

(Received May 29, 2015, Revised December 17, 2015, Accepted December 19, 2015)

Abstract. Strip footing is an important type of shallow foundations and is commonly used beneath the walls. Analysis of shallow foundation involves the determination of stresses and deformations. Element free Galerkin method, one of the important mesh free methods, is used for the determination of stresses and deformations. Element free Galerkin method is an efficient and accurate method as compared to finite element method. The Element Free Galerkin method uses only a set of nodes and a description of model boundary is required to generate the discrete equation. Strip footing of width 2 m subjected to a loading intensity of 200 kPa is studied. The results obtained are agreeing with the values obtained using analytical solutions available in the literature. Parametric study is done and the effect of modulus of deformation, Poisson's ratio and scaling parameter on deformation and stresses are determined.

Keywords: strip footing; mesh free; element free galerkin method; vertical deformations; stress distribution

1. Introduction

Shallow foundations are one of the important classes of structural foundations. A shallow foundation transmits structural loads to the soil strata at relatively small depths. Terzaghi defined a shallow foundation as the one which is laid at a depth D_f such that D_f is smaller than width of foundation.

The estimation of settlement and stress distribution of shallow foundations is an important topic in the design and construction of buildings and other related structures. In general, settlement of a foundation consists of two major components—elastic settlement (S_e) and consolidation settlement (S_c) (Ranjan and Rao 2011). In turn, the consolidation settlement of a submerged clay layer has two parts; that is, the contribution of primary consolidation settlement (S_p) and that due to secondary consolidation (S_s) (Ranjan and Rao 2011). For a foundation supported by granular soil within the zone of influence of stress distribution, the elastic settlement is the only component that needs consideration.

In the present study element free Galerkin method (EFGM) is used to determine the settlements and stress distribution beneath a strip or continuous footing. Meshfree method is a method used to

*Corresponding author, Associate Professor, E-mail: sawntf@iitr.ac.in

^aM Tech student, E-mail: aashiqganaie1991@gmail.com

establish system of algebraic equations for the whole problem domain without the use of a predefined mesh for the domain discretization (Belytschko 1994, Dolbow and Belytschko 1998, Park and Leap 2000, Liu and Gu 2005, Kumar and Dodagoudar 2010, Mategaonkar and Eldho 2011, Mategaonkar and Eldho 2012, Thomas *et al.* 2013, Pandey *et al.* 2013). EFGM is a Meshfree method developed recently to eliminate the structure of mesh and construct approximate solutions for the equation in terms of nodes. EFGM is used to model the governing differential equation for deformations and a methodology is proposed for two dimensional deformation phenomenon. The model is further extended for conducting parametric study to examine the effect of material constants on the deformation behaviour of soil. Plane strain condition is considered in the study.

2. Description of the problem

In this study a strip footing of width, $B=2$ m is taken which is subjected to a loading intensity of $q=0.2$ MPa as shown in Fig. 1. Due to symmetry, deformations and stress distribution of only one side of footing are evaluated taking centre of the footing as origin. Deformations and stresses up to a depth equal to $5B$ and also up to a horizontal distance equal to $5B$ are determined using the EFGM. This domain is represented by nodes placed in a regular arrangement. The nodes are placed at a distance of $0.5B$, both in vertical and horizontal direction. Thus there are 121 nodes, out of which 31 nodes are placed on the boundary surfaces. These sets of scattered nodes are called *field nodes*, and they do not form a mesh. Part of upper surface represents the traction boundary and total number of nodes on traction boundary is 2.

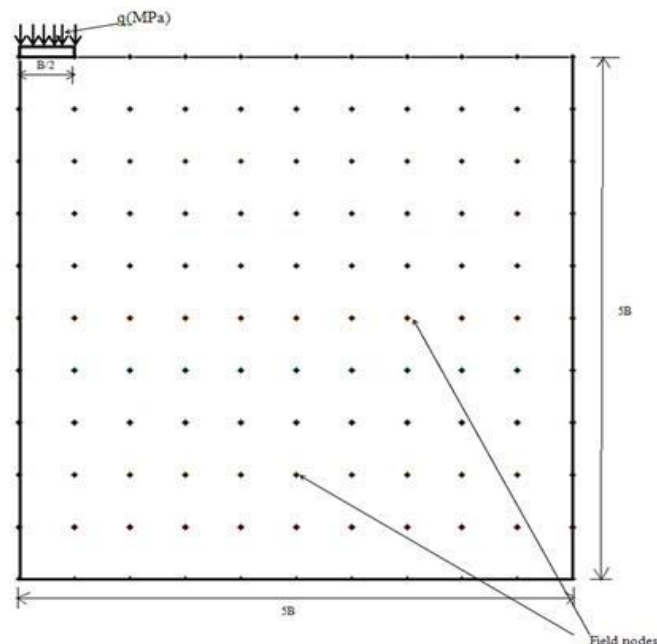


Fig. 1 Strip footing with loading intensity of q (MPa) and distribution of nodes

3. Element free Galerkin method

Belytschko *et al.* (1994) proposed the EFGM in which the moving least squares (MLS) approximation, was used in the Galerkin weak-form to establish a set of algebraic equations. The MLS approximations are based upon a weight function, a polynomial basis, and a set of coefficients (Belytschko 1994, Dolbow and Belytschko 1998, Park and Leap 2000, Wang and Li 2006). EFGM employs MLS approximants to approximate the function $U(X)$ with $U^h(X)$ in which $U(x)$ is the deformation vector at x , where x is a position vector as $x^T = (x,y)$. EFGM do not satisfy the Kronecker delta criterion and hence Lagrangian multiplier technique (Dolbow and Belytschko 1998) is used to enforce the Dirichlet boundary condition (Dolbow and Belytschko 1998, Kumar and Dodagoudar 2010). In the EFGM, the problem domain is represented by a set of properly distributed nodes.

Moving least squares approximations

As per the moving least square approximants, the approximation $U^h(x)$ of $U(x)$ is given (Dolbow and Belytschko 1998, Belytschko *et al.* 1995) as

$$U(x) = U^h(x) = \sum_{i=1}^m p_i(x)a_i(x) = P^T(x)a(x) \quad \forall x \in \Omega \quad (1)$$

In which

$$P^T(x) = [1 \ x \ y] \text{ and } a^T(x) = [a_0(x), a_1(x), a_2(x), \dots, a_m(x)] \quad (2)$$

Where $P(x)$ is the basis function of spatial coordinates, $x^T=[x, y]$ for two dimensional problem in domain Ω , and m is the number of the basis functions. $a(x)$ is a vector of undetermined coefficients and whose values depend on the of position vector x . These coefficients can be obtained by minimizing the following weighted discrete **L2** norm (Dolbow and Belytschko 1998, Belytschko *et al.* 1995).

$$J = \sum_{i=1}^n W(x-x_i) [P^T(x)a(x) - U_i]^2 \quad (3)$$

where $W(x-x_i)$ is the weight function associated with the nodal point x_i in the domain Ω and n is a local node number whose support includes x or n is the number of nodes in neighbourhood of x for which weight function $W(x-x_i)$ is non-zero and U_i refers to nodal parameter of U at $x = x_i$.

Minimizing J with respect to $a(x)$ leads to the following set of linear equations

$$A(x)a(x) = B(x)U \quad (4)$$

$$a(x) = A^{-1}(x)B(x)U \quad (5)$$

where

$$A(x) = \sum_{i=1}^n W(x-x_i)P(x_i)P^T(x_i)$$

$$= W(x-x_1) \begin{bmatrix} 1 & x_1 & y_1 \\ x_1 & x_1^2 & x_1 y_1 \\ y_1 & x_1 y_1 & y_1^2 \end{bmatrix} + \dots + W(x-x_n) \begin{bmatrix} 1 & x_n & y_n \\ x_n & x_n^2 & x_n y_n \\ y_n & x_n y_n & y_n^2 \end{bmatrix} \tag{6}$$

$$B(x) = [W(x-x_1)P(x_1), W(x-x_2)P(x_2), \dots, W(x-x_n)P(x_n)]$$

$$= W(x-x_1) \begin{bmatrix} 1 \\ x_1 \\ y_1 \end{bmatrix}, W(x-x_2) \begin{bmatrix} 1 \\ x_2 \\ y_2 \end{bmatrix}, \dots, W(x-x_n) \begin{bmatrix} 1 \\ x_n \\ y_n \end{bmatrix} \tag{7}$$

$$U^T = [U_1, U_2, U_3, \dots, U_n] \tag{8}$$

By substituting Eq. (5) in Eq. (1), the MLS approximate for $U(\mathbf{x})$ is

$$U(x) \cong U^h(x) = \sum_{i=1}^n (P^T(x)A^{-1}(x)B(x)U) = \sum_{i=1}^n \phi_i(x)U = \Phi U \tag{9}$$

where

$$\phi_i(x) = P^T(x)A^{-1}(x)B(x) \quad \text{and} \quad \Phi = [\phi_1, \phi_2, \phi_3, \dots, \phi_n] \tag{10}$$

According to Belytschko *et al.* (1996), the shape functions can be written as

$$\phi_i(x) = P^T(x)A^{-1}(x)B_i(x) = \psi^T(x)B_i(x) \tag{11}$$

which leads to the relationship

$$A(x)\psi(x) = P(x) = [1 \quad x \quad y]^T \tag{12}$$

Differentiating Eq. (12) with respect to \mathbf{x} , the following is obtained

$$A(x)\psi_{,x}(x) + A_{,x}(x)\psi(x) = P_{,x}(x) \tag{13a}$$

$$A(x)\psi_{,x}(x) + A_{,x}(x)\psi(x) = P_{,x}(x) = [0 \quad 1 \quad 0]^T \tag{13b}$$

$$A_{,y}(x)\psi(x) + A(x)\psi_{,y}(x) = P_{,y}(x) = [0 \quad 0 \quad 1]^T \tag{13c}$$

The vector $\psi(\mathbf{x})$ is determined using an LU decomposition of the matrix \mathbf{A} in Eq. (12) followed by back substitution. Eq. (13(a)) can be rearranged as

$$A(x)\psi_{,x}(x) = P_{,x}(x) - A_{,x}(x)\psi(x) \tag{14}$$

The derivative of $\psi(\mathbf{x})$ can be calculated using the same LU decomposition obtained from Eq. (12). This leads to a simple relationship for the spatial derivative of the EFGM shape function of node i in Eq. (11) and is given as:

$$\phi_{i,x}(x) = \psi^T_{,x}(x)B_i(x) + \psi^T(x)B_{i,x}(x) \tag{15}$$

Where

$$B_{i,x} = \frac{d}{dx} W(x - x_i) P(x_i) \tag{16}$$

Weight function description

The weight function is non-zero over a small neighbourhood of x_i , called support domains. In the reported studies so far, weight function $W(\mathbf{x}-\mathbf{x}_i)$ is always chosen to have the following properties (Liu and Gu 2005, Dolbow and Belytschko 1998, Park and Leap 2000):

- $W(\mathbf{x}-\mathbf{x}_i) > 0$ within the support domain.
- $W(\mathbf{x}-\mathbf{x}_i) = 0$ outside the support domain.
- $W(\mathbf{x}-\mathbf{x}_i)$ monotonically decreases from the point of interest at \mathbf{x} .
- $W(\mathbf{x}-\mathbf{x}_i)$ is sufficient smooth, especially on the boundary of domain Ω_s .

In the present study tensor product weights will be used with the quartic spline function used for implementation of the method in two dimensions

$$W(x - x_i) = W(r_x)W(r_y) \tag{17}$$

Where

$$r_x = \|x - x_i\| / d_{mx} \tag{18}$$

$$r_y = \|y - y_i\| / d_{my} \tag{19}$$

Where

$$d_{mx} = d_{\max} x_{spac} \tag{20}$$

$$d_{my} = d_{\max} y_{spac} \tag{21}$$

Where x_{spac} and y_{spac} gives the average spacing between the nodes in x and y direction and d_{\max} is a scaling parameter which is typically 2.0-4.0 for static analysis. The distance x_{spac} and y_{spac} is determined by searching for enough neighbour nodes for A to be regular.

The tensor weight functions will be given as (Liu and Gu 2005)

$$W(r_x) = \begin{cases} 1 - 6r_x^2 + 8r_x^3 - 3r_x^4 & r_x \leq 1 \\ 0 & r_x > 1 \end{cases} \tag{22}$$

and

$$W(r_y) = \begin{cases} 1 - 6r_y^2 + 8r_y^3 - 3r_y^4 & r_y \leq 1 \\ 0 & r_y > 1 \end{cases} \tag{23}$$

Enforcement of essential boundary conditions

Since in the EFGM the shape functions do not fulfill the Kronecker delta condition (i.e.,

$\phi_i(x_j) \neq \delta_{ij}$), the enforcement of Dirichlet (or essential) boundary conditions is not straightforward, but requires special methods. Among them the most common ones are the Lagrange multipliers method, modified variational principles, penalty methods, coupling with finite elements (Liu and Gu 2005) etc. In this study, the Lagrange multiplier method is used to enforce the essential boundary conditions in the EFGM.

4. Equilibrium equations and EFG numerical implementation

As is well-known the equilibrium of a body that occupies the domain Ω bounded by surface Γ can be stated mathematically as follows (Liu and Gu 2005, Dolbow and Belytschko 1998)

$$\nabla \cdot \boldsymbol{\sigma} + \mathbf{b} = 0 \quad (24)$$

where $\boldsymbol{\sigma}$ is the stress tensor, which corresponds to the displacement field \mathbf{u} and \mathbf{b} is a body force vector. The boundary conditions are as follows (Dolbow and Belytschko 1998)

$$\boldsymbol{\sigma} \cdot \mathbf{n} = \bar{\mathbf{t}} \quad \text{on } \Gamma_t \quad (25)$$

and

$$\mathbf{u} = \bar{\mathbf{u}} \quad \text{on } \Gamma_u \quad (26)$$

Where $\bar{\mathbf{t}}$ and $\bar{\mathbf{u}}$ represent the given traction and displacements on the portion Γ_t and Γ_u of the boundary respectively and \mathbf{n} is a unit vector normal to domain Ω .

The minimum total potential energy is applied and the following Galerkin weak-form can be obtained (Brighenti 2005)

$$\delta \Pi = \frac{1}{2} \int_{\Omega} \delta \boldsymbol{\varepsilon}^T \boldsymbol{\sigma} d\Omega - \int_{\Omega} \delta \mathbf{u}^T \mathbf{b} d\Omega - \int_{\Gamma_t} \delta \mathbf{u}^T \bar{\mathbf{t}} d\Gamma = 0 \quad (27)$$

In order to evaluate the integrals in Eq. (27), the global problem domain Ω is discretized into a set of the so-called background cells that are not overlapping.

Making the use of stress-strain relations, strain- displacement relations and $\mathbf{u} = \boldsymbol{\phi}_I \mathbf{u}_I$ Eq. (27) can be written as

$$\delta \mathbf{U}^T [\mathbf{K} \mathbf{U} - \mathbf{F}] = 0, \quad \mathbf{F} = \mathbf{F}^b + \mathbf{F}^t \quad (28)$$

Where

$$\mathbf{K}_{IJ} = \int_{\Omega} (\mathbf{B}_I^T)_{2 \times 3} \mathbf{D}_{3 \times 3} (\mathbf{B}_J)_{3 \times 2} d\Omega \quad (29)$$

$$\mathbf{F}_I^b = \int_{\Omega} \boldsymbol{\phi}_I^T \mathbf{b} d\Omega \quad (30)$$

And

$$F_I^t = \int_{\Gamma_I} \phi_I^T \bar{t} d\Gamma_I \tag{31}$$

K_{II} is the nodal stiffness matrix and \mathbf{K} is the global stiffness matrix assembled using nodal stiffness matrices of all nodes in the entire problem domain and the dimension of \mathbf{K} matrix is $(2N \times 2N)$. F_I^b is the nodal body force vector and \mathbf{b} is the body force vector and F^b is the global body force vector assembled using the nodal body force vectors for all nodes in the entire problem domain and the dimension of F^b matrix is $(2N \times 1)$. F_I^t is the nodal traction force vector and F^t is the global traction force vector assembled using the nodal traction force vectors. The length of vector F^t should be $(2N \times 1)$.

D is an elastic constitutive matrix and for plane strain condition, it is given as

$$D = \frac{E}{(1+\nu)(1-2\nu)} \begin{bmatrix} 1-\nu & \nu & 0 \\ \nu & 1-\nu & 0 \\ 0 & 0 & 1-2\nu \end{bmatrix} \tag{32}$$

Lagrange multiplier method is used for imposing essential boundary conditions and this method is briefly explained below.

The functional related to the essential boundary condition, $(u = \bar{u})$, is written in an integral form using the Lagrange multiplier λ (Liu and Gu 2005, Dolbow and Belytschko 1998)

$$\int_{\Gamma_u} \lambda^T (u - \bar{u}) d\Gamma$$

The constrained galerkin weak form can then be re-written as (Liu and Gu 2005)

$$\int_{\Omega} L(\delta u)^T (DLu) d\Omega - \int_{\Omega} \delta u^T b d\Omega - \int_{\Gamma_I} \delta u^T \bar{t} d\Gamma - \int_{\Gamma_u} \delta \lambda^T (u - \bar{u}) d\Gamma - \int_{\Gamma_u} \delta u^T \lambda d\Gamma = 0 \tag{33}$$

In order to obtain the discretized formulation, the Lagrange multipliers λ in Eq. (33), need to be interpolated using their nodal values and shape functions for nodes on the essential boundaries (Liu and Gu 2005).

$$\lambda^T = N(s)_{2 \times 2n_\lambda} \lambda_{2n_\lambda \times 1} \tag{34}$$

Where n_λ is the number of nodes used for this interpolation, N_I is the shape function for the I^{th} node on the essential boundary, s is the arc-length along the essential boundary, λ is the vector of the nodal Lagrange multipliers of field nodes on the essential boundary. Using Lagrange multiplier the final equation is given as (Liu and Gu 2005, Dolbow and Belytschko 1998).

$$\delta U^T [\mathbf{K}U + \mathbf{G}\Lambda - \mathbf{F}] + \delta \Lambda^T (\mathbf{G}^T U - \mathbf{Q}) = 0 \tag{35}$$

\mathbf{G} is the global matrix formed by assembling \mathbf{G}_{II} and \mathbf{Q} is the global vector formed by assembling \mathbf{q}_I (Liu and Gu 2005, Dolbow and Belytschko 1998).

$$\mathbf{G}_{\mathbf{U}} = - \int_{\Gamma_u} \phi_I^T N_J d\Gamma \quad \backslash \quad (36)$$

And

$$q_I = - \int_{\Gamma_u} N_I^T \bar{u} d\Gamma \quad (37)$$

Because both $\delta\mathbf{U}$ and $\delta\mathbf{\Lambda}$ are arbitrary, this equation can be satisfied only if

$$\mathbf{K}\mathbf{U} + \mathbf{G}\mathbf{\Lambda} - \mathbf{F} = 0$$

$$\mathbf{G}^T\mathbf{U} - \mathbf{Q} = 0$$

The above equations can be written in matrix form as (Liu and Gu 2005, Dolbow and Belytschko 1998)

$$\begin{bmatrix} \mathbf{K} & \mathbf{G} \\ \mathbf{G}^T & 0 \end{bmatrix}_{(2N+2n_\lambda) \times (2N+2n_\lambda)} \begin{bmatrix} \mathbf{U} \\ \mathbf{\Lambda} \end{bmatrix}_{(2N+2n_\lambda) \times 1} = \begin{bmatrix} \mathbf{F} \\ \mathbf{Q} \end{bmatrix}_{(2N+2n_\lambda) \times 1} \quad (38)$$

Eq. (38) is the final discretized system equations for the EFG method using the Lagrange multiplier method. Solving Eq. (38) gives the results of nodal parameters of the displacements (deformations) for this problem, and the displacements at any point including at the field nodes in the problem domain can be obtained using Eq. (9).

5. Results and discussions

Since in the strip footing, length (L) is very large as compared to width (B) of footing, plane strain condition is considered and thus the elastic constitutive matrix (D) for plane strain condition is given by Eq. (32). The effect of strip footing is considered up to a depth of $5B$ in vertical direction and up to a length of $5B$ in horizontal direction. Thus a domain which is considered for the analysis is a square in shape and having size $5B \times 5B$. The nodes are distributed regularly. The domain is represented by nodes which are at a spacing of $0.5B$ from each other in both vertical and horizontal direction. The background cells which are used for numerical integration are obtained by dividing the domain into 10 divisions in both vertical and horizontal direction and a mesh of background cells of size $0.5B \times 0.5B$ is obtained. A program in FORTRAN using meshfree numerical technique is written for the determination of deformations and stresses in the domain considered above. The following boundary conditions are considered in the analysis:

- 1) The horizontal deformations, on the surface (plane) passing through the centre of strip footing in vertical direction, are zero.
- 2) The vertical deformations, on the surface (plane) passing through the bottom of the domain considered for analysis (at a depth of $5B$) in horizontal direction, are zero.
- 3) The horizontal deformations, on the surface (plane) at a distance of $5B$ from centre of footing and passing in vertical direction, are zero.

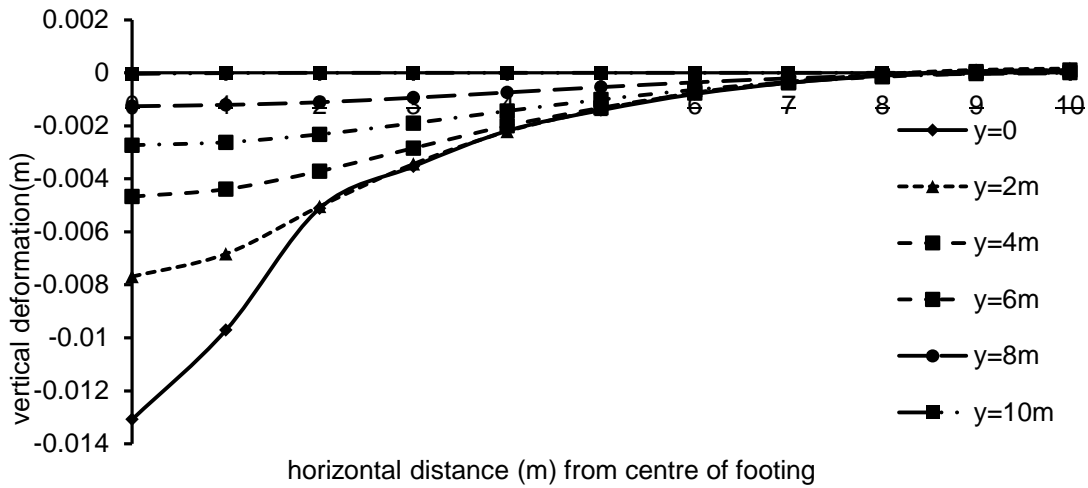


Fig. 2 Variation of vertical deformation with horizontal distance from centre of footing at various depths below the surface

5.1 Deformation profiles

The vertical deformations at different horizontal surfaces and horizontal deformations at different vertical surfaces are shown in Figs. 2 and 3 respectively. The modulus of deformation (E) is taken equal to 50 MPa and Poisson ratio (ν) of 0.3 is considered. In the Fig. 2 vertical settlements at depths varying from 0 to 10 m at intervals of 2 m are represented. It is evident from Fig. 2 that settlements keep on decreasing with increase in depth and horizontal distance from footing. At depth of 10 m (bottom surface) vertical deformations are zero as shown in Fig. 2 and thus the boundary condition is satisfied.

Fig. 3 represents the horizontal deformations at distances ranging from 0 to 10 m, at intervals of 2 m, from centre of footing. At centre ($x=0$) and at a distance of 10 m from centre ($x=10$ m), horizontal deformations are zero as shown in Fig. 3 and thus the boundary conditions are satisfied. The horizontal deformation initially increases with distance in horizontal direction and reduces thereafter. The horizontal deformation reduces with depth for all distances from centre of footing.

The following analytical formula has been used for the calculation of relative vertical displacement (Das 2008, Poulos and Davis 1974)

$$w_{z=0(x)} - w_{z=0(x=0)} = \frac{2q(1-\nu^2)}{\pi E} \left\{ (x-b)\ln|x-b| - (x+b)\ln|x+b| + 2b\ln(b) \right\} \quad (39)$$

The vertical deformations at the surface have been validated for different values of modulus of deformation (E) and the results are shown in Fig. 4. From these plots, it looks that vertical deformations at the surface agree very well with analytical one initially with horizontal distance and after a distance of 5 m from footing, the analytical deformations become more as compared to that determined from EFGM. These relative deformations are determined for modulus of deformations (E) of 25 MPa, 50 MPa, 75 MPa and 95 MPa. The Poisson ratio (ν) was 0.4 for all the cases.

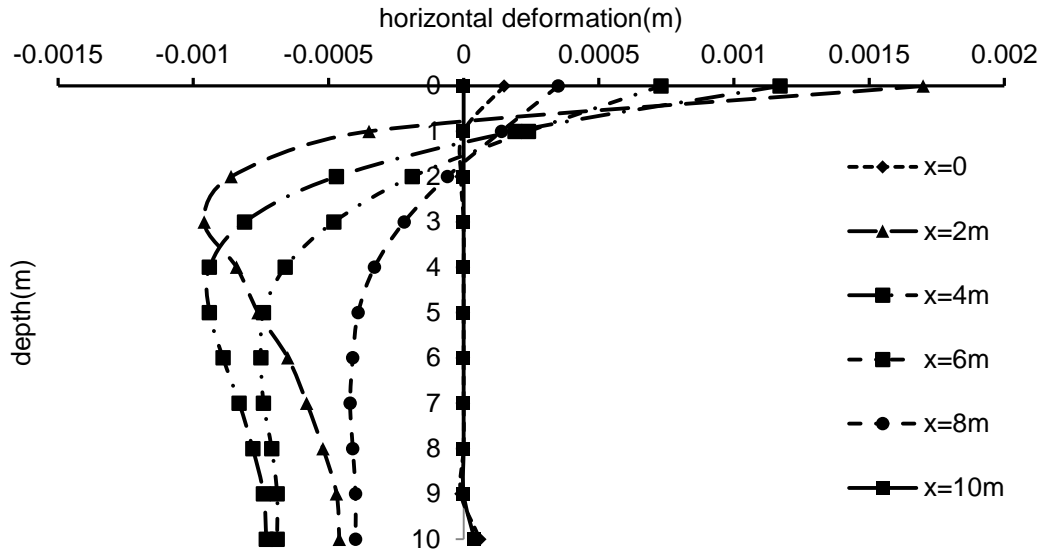


Fig. 3 Variation of horizontal deformation with depth at various distances from centre of footing

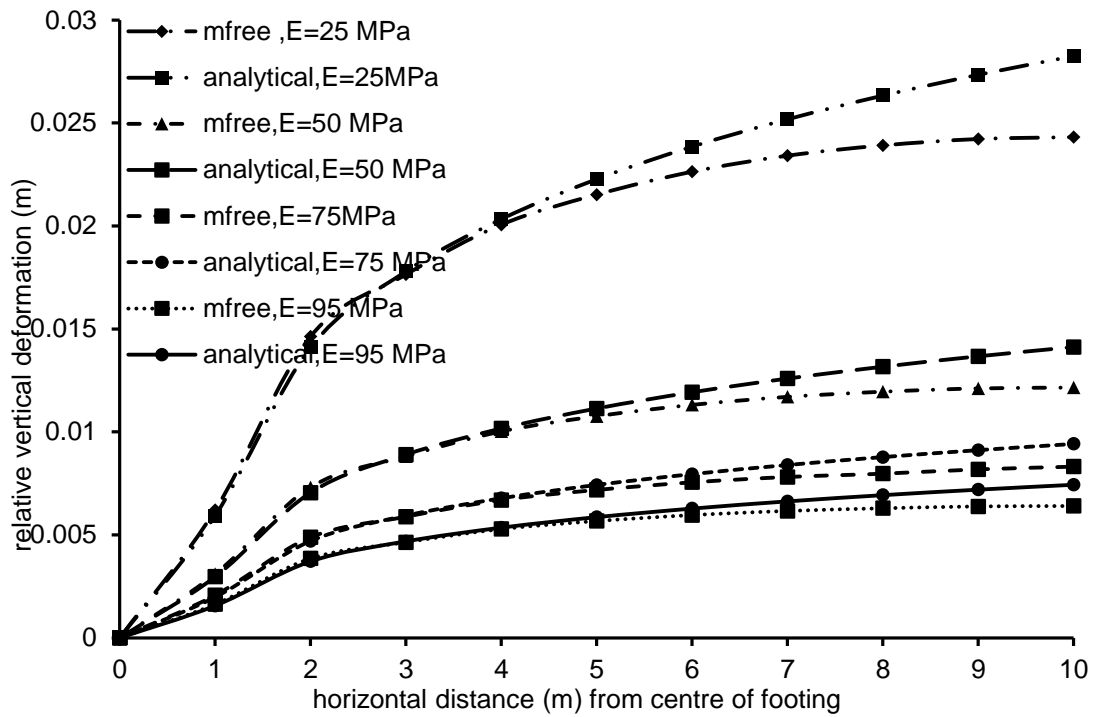


Fig. 4 Comparison of relative vertical deformations as determined by EFGM and by analytical solutions for different values of E and $\nu=0.4$

5.2 Distribution of stresses

Plots have been drawn for vertical and horizontal stresses with depth for various distances from centre of footing. Fig. 5 shows the variation of vertical stress with depth for various distances x from centre of footing of width $B=2$ m, subjected to a loading intensity, $q=0.2$ MPa. From Fig. 5, it is observed that vertical stresses developed by the load keeps on decreasing with depth and as depth becomes more this decrease in vertical stress becomes smaller and smaller. At depths greater than 8 m ($4B$), they remain constant. Similarly as distance from footing increases in horizontal direction, stresses keep on reducing. Same behaviour is shown by horizontal stresses.

Fig. 6 shows the validation of vertical stresses with the analytical solution available in the literature (Das 2008, Poulos and Davis 1974). These plots show that results obtained from both these methods agree with marginal deviations.

6. Parametric study

After assuring the accuracy of the program, study is extended to examine the effect of modulus of elasticity, Poisson ratio and scaling parameter (d_{max}) on deformation and on stresses.

6.1 Effect of modulus of deformation (E)

Vertical deformation of the top surface and horizontal deformation of vertical plane at 1 m from centre are presented in Figs. 7 and 8 for different modulus of deformation E . From Figs. 7 and 8, it is observed that deformations decrease with increase in the value of modulus of deformation (E). Maximum vertical deflection ($E = 25$ MPa) is 22.37 mm.

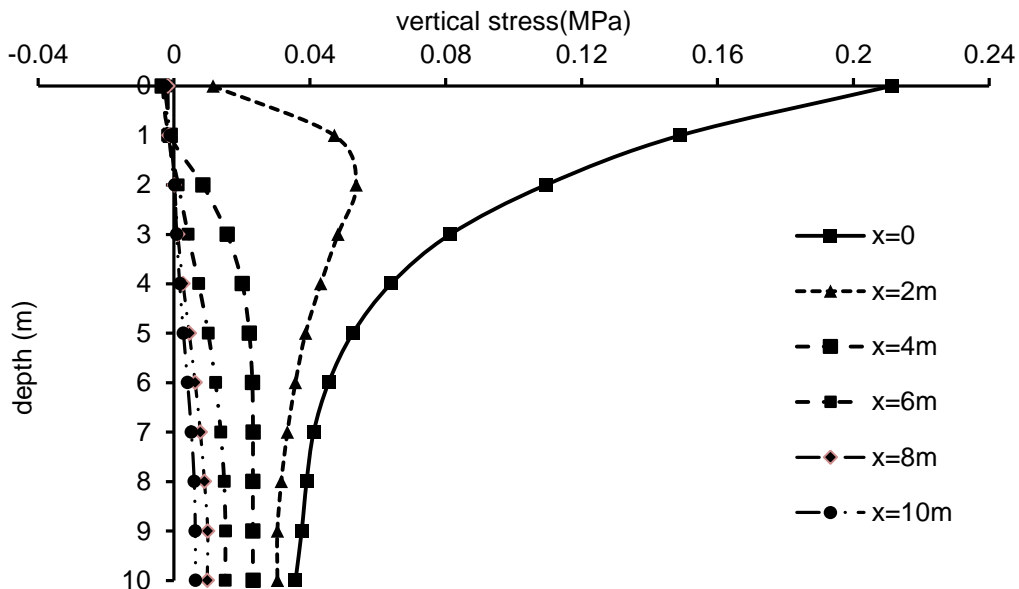


Fig. 5 Variation of vertical stress (σ_v) with depth for different distances from centre of footing for $E=50$ MPa and $\nu=0.4$

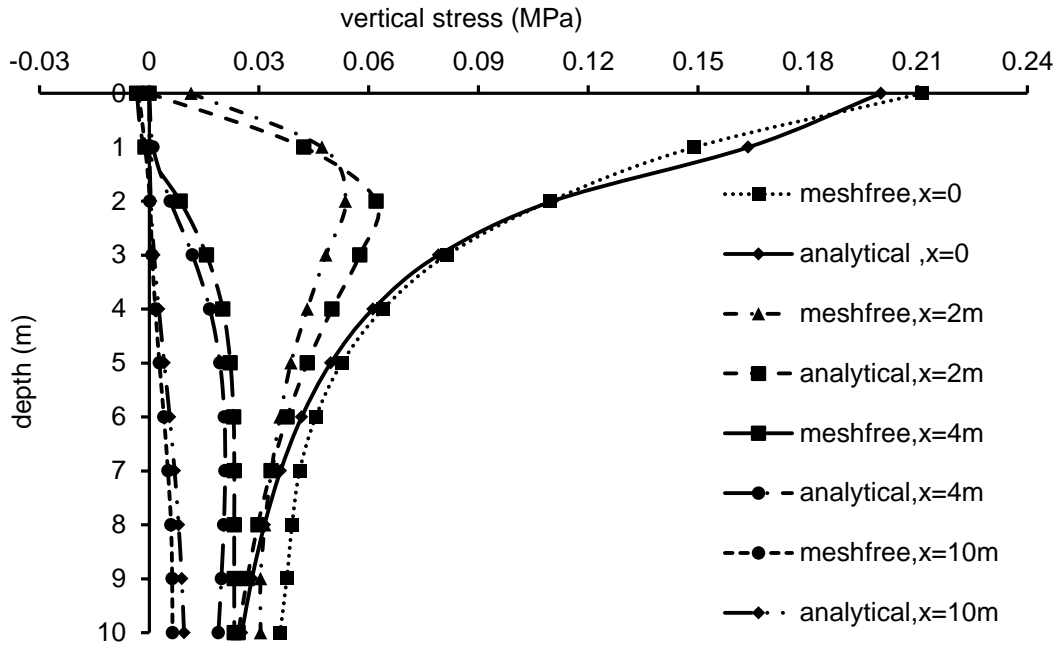


Fig. 6 Comparison of vertical stress (σ_v) determined using EFGM and by analytical solutions, for different distances from centre of footing for $E=50$ MPa and $\nu=0.4$

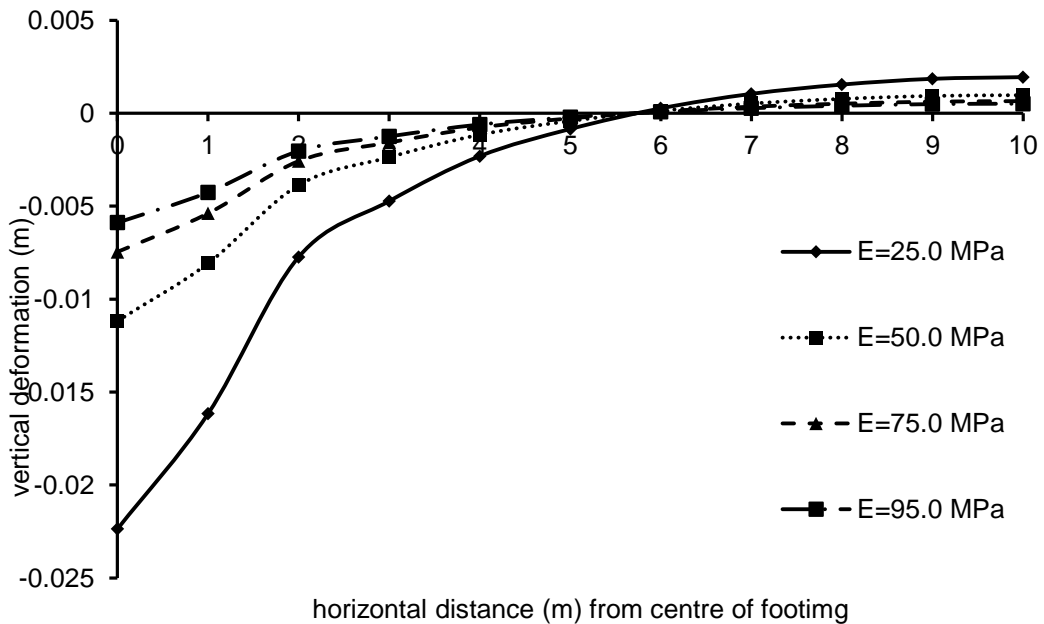


Fig. 7 Variation of vertical deformation at the surface with horizontal distance from centre of footing, for various values of modulus of deformation (E)

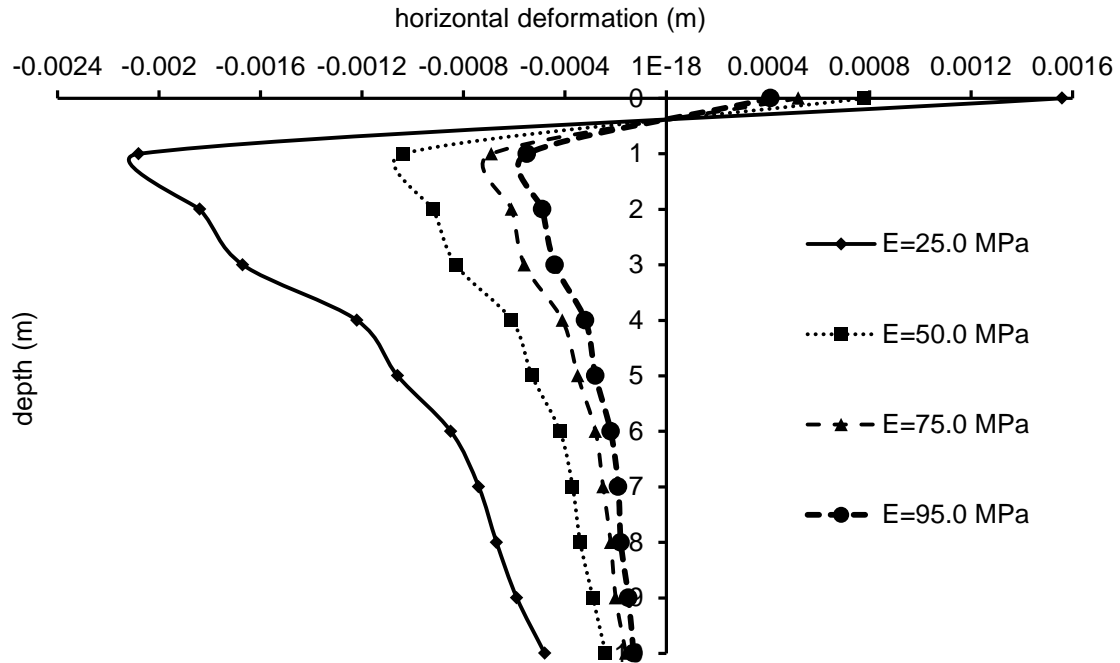


Fig. 8 Variation of horizontal deformation at distance $x=1\text{m}$ from centre of footing with depth below the surface of footing, for various values of modulus of deformation (E)

With increase in modulus, reduction is of the order of 50.02% ($E = 50\text{ MPa}$), 66.65% ($E = 75\text{ MPa}$) and 73.67% ($E = 95\text{ MPa}$). Maximum horizontal displacement ($E = 25\text{ MPa}$) is 2.08 mm. With increase in modulus, reduction is of the order of 50.0% ($E = 50\text{ MPa}$), 66.8% ($E = 75\text{ MPa}$) and 73.5% ($E = 95\text{ MPa}$).

On the contrary, horizontal and vertical stress distribution reported negligible effect on the distribution of stresses with change in modulus.

6.2 Effect of poisson ratio (ν)

Vertical deformation of the top surface and horizontal deformation of vertical plane at 1 m from centre are presented in Figs. 9 and 10 for different values of Poisson ratio (ν). From Fig. 9, it is observed that vertical displacement decrease with increase in the value of Poisson ratio (ν). Maximum vertical deflection ($\nu = 0.25$) is 13.76 mm. With increase in Poisson ratio, reduction is of the order of 4.94% ($\nu = 0.30$), 11.05% ($\nu = 0.35$), 18.75% ($\nu = 0.40$) and 28.12% ($\nu = 0.45$). From Fig. 10, it is observed that horizontal displacement increases with increase in the value of Poisson ratio (ν). Maximum horizontal deflection ($\nu = 0.45$) is 1.25 mm. With decrease in Poisson ratio, reduction is of the order of 16.8% ($\nu = 0.40$), 33.6% ($\nu = 0.35$), 49.6% ($\nu = 0.30$) and 65.6% ($\nu = 0.25$).

Variation of vertical and horizontal stress with depth, on a vertical plane passing through centre of footing, for different values of Poisson ratio (ν) are presented in Figs. 11 and 12. From these

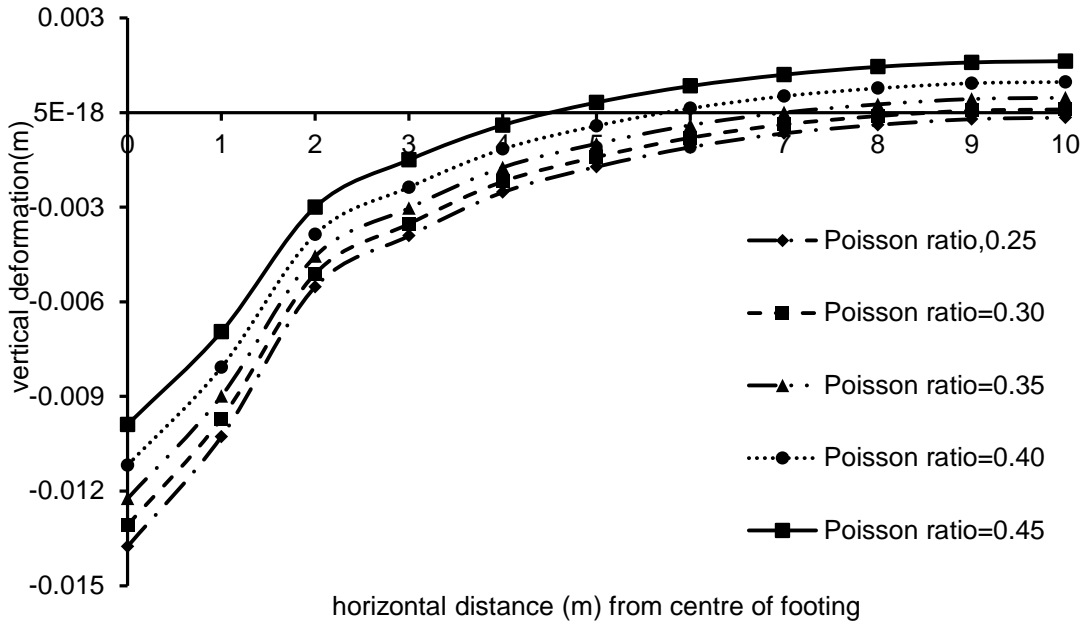


Fig. 9 Variation of vertical deformation at the surface with horizontal distance from centre of footing, for various values of Poisson ratio (ν)

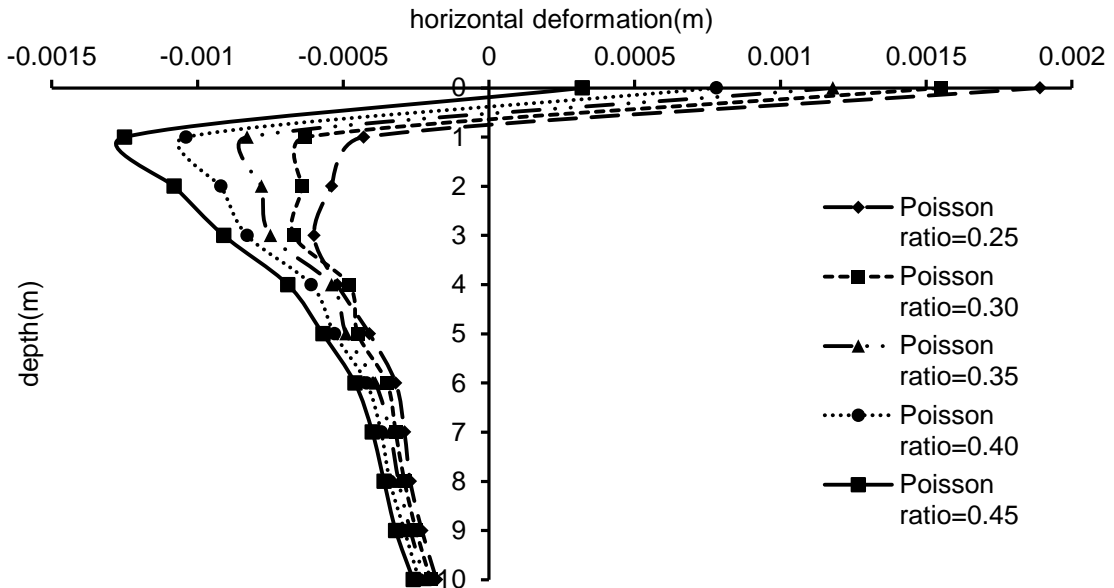


Fig. 10 Variation of horizontal deformation with depth at the distance of 1m from centre of footing, for various values of Poisson ratio (ν)

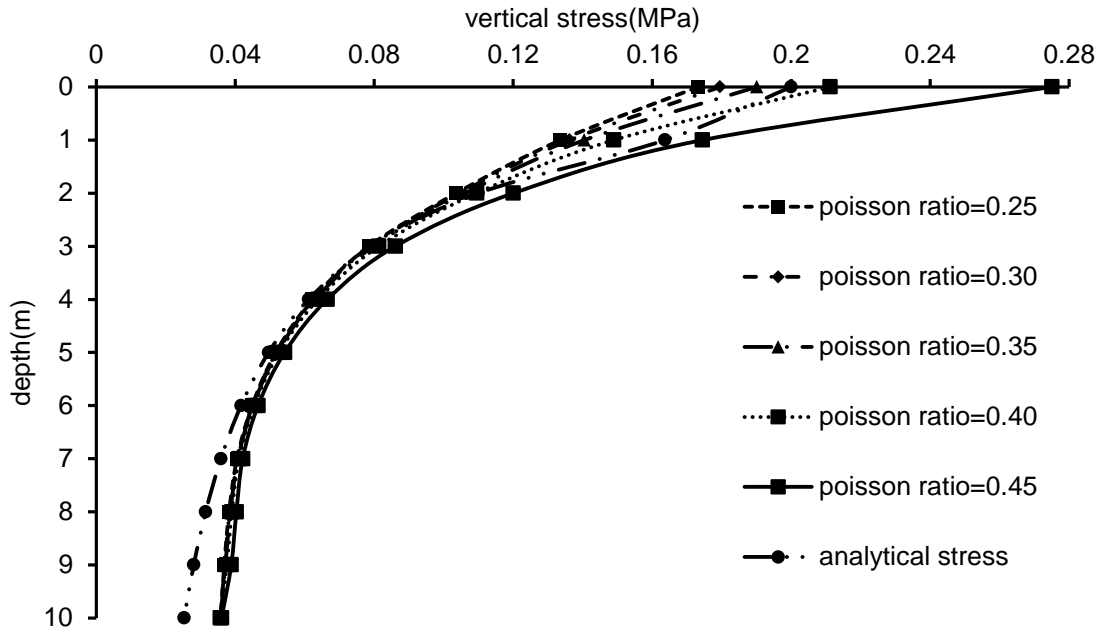


Fig. 11 Variation of vertical stress with depth, on a vertical plane passing through centre of footing, for different values of Poisson ratio (ν)

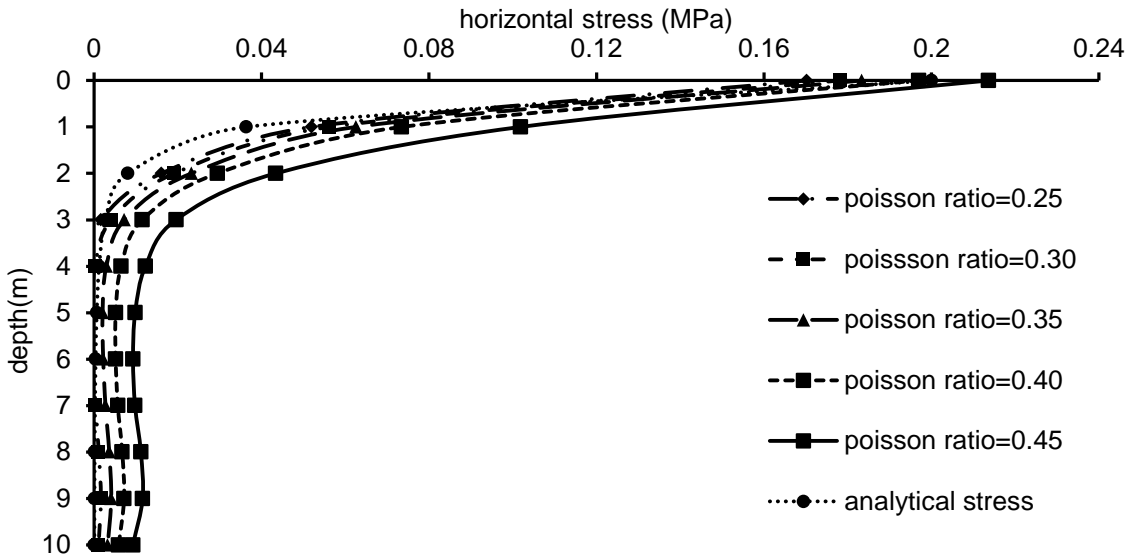


Fig. 12 Variation of horizontal stress with depth, on a vertical plane passing through centre of footing, for different values of Poisson ratio (ν)

Figs., it is observed that with increase in Poisson ratio, there is an increase in both vertical and horizontal stress. Similar effects are observed on other vertical planes at different distances from centre of footing. With increase in depth, variation in stresses for different values of ν reduces and below a depth of $2B$ vertical stress remains constant for all values of Poisson ratio. Maximum value of vertical stress ($\nu = 0.45$) is 275 kPa. With decrease in Poisson ratio, reduction is of the order of 23.2% ($\nu = 0.40$), 30.9% ($\nu = 0.35$), 34.5% ($\nu = 0.30$) and 37.0% ($\nu = 0.25$). Maximum value of horizontal stress ($\nu = 0.45$) is 213.4 kPa. With decrease in Poisson ratio, reduction is of the order of 6.1% ($\nu = 0.40$), 14.1% ($\nu = 0.35$), 16.5% ($\nu = 0.30$) and 20.1% ($\nu = 0.25$).

6.3 Effect of scaling parameter (d_{max})

Figs. 13 and 14 show the variation of vertical and horizontal stress with depth, on a vertical plane at the centre of footing, for different values of scaling parameter (d_{max}). It is observed that d_{max} do not have a significant influence on stress distribution especially as depth keeps on increasing. At shallow depths, higher values of stress are for smaller values of d_{max} . Maximum value of vertical stress ($d_{max} = 2.0$) is 222.5 kPa. With increase in scaling parameter, decrease in vertical stress is of the order of 3.14% ($d_{max} = 2.5$), 5.07% ($d_{max} = 3.0$), 12.4% ($d_{max} = 3.5$), 19.7% ($d_{max} = 4.0$). Maximum value of horizontal stress ($d_{max} = 2.0$) is 213.25kPa. With increase in scaling parameter, decrease in horizontal stress is of the order of 5.71% ($d_{max} = 2.5$), 7.64% ($d_{max} = 3.0$), 11.61% ($d_{max} = 3.5$), 14.44% ($d_{max} = 4.0$). Fig. 15 shows vertical deformation of the top surface for different scaling parameters (d_{max}). It is observed that d_{max} have no influence on deformations. Same is the case with horizontal deformations.

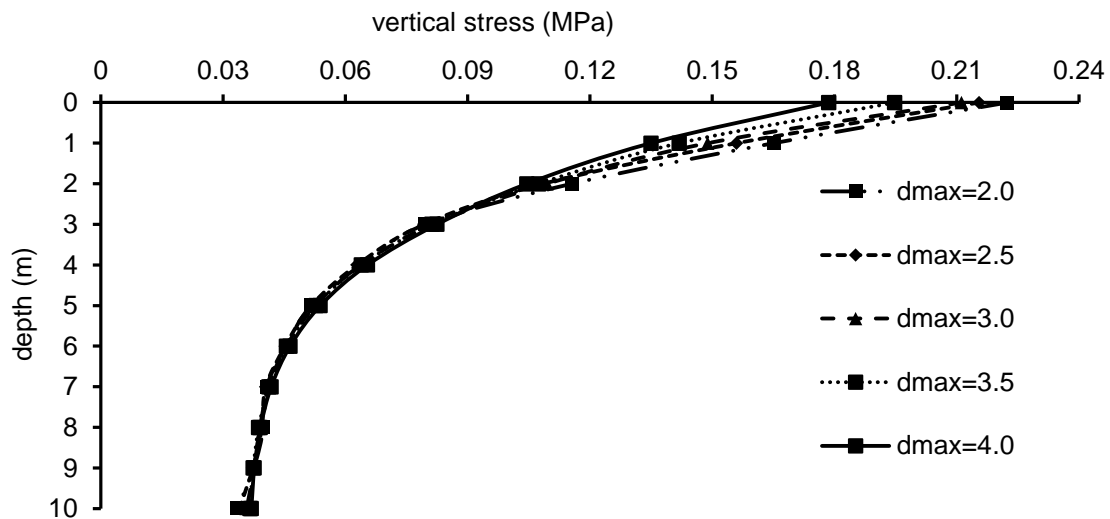


Fig. 13 Variation of vertical stress with depth, on a vertical plane passing through centre of footing, for different values of scaling parameter (d_{max})

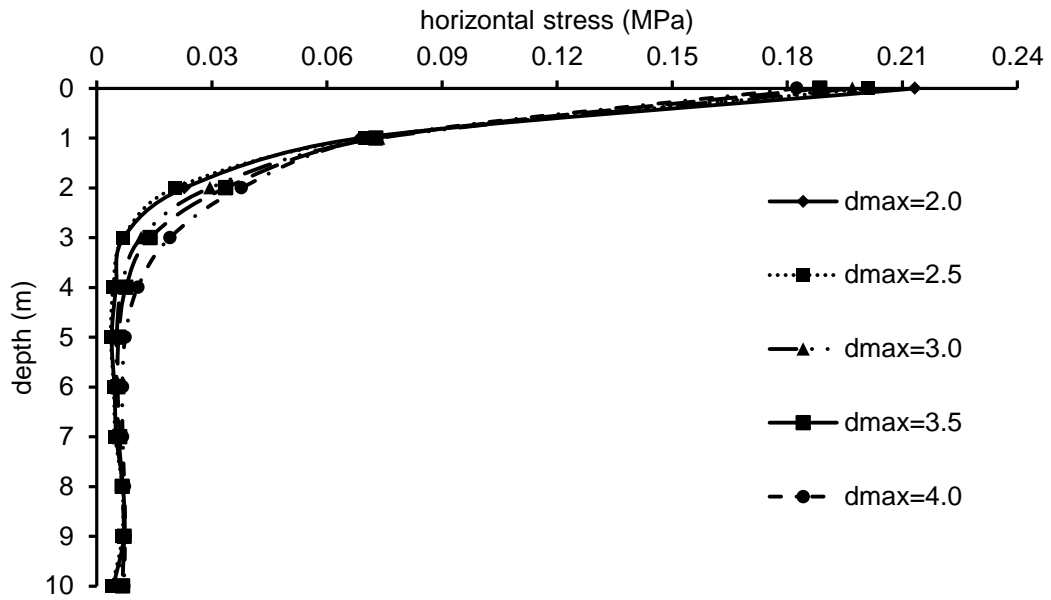


Fig. 14 Variation of horizontal stress with depth, on a vertical plane passing through centre of footing, for different values of scaling parameter (d_{max})

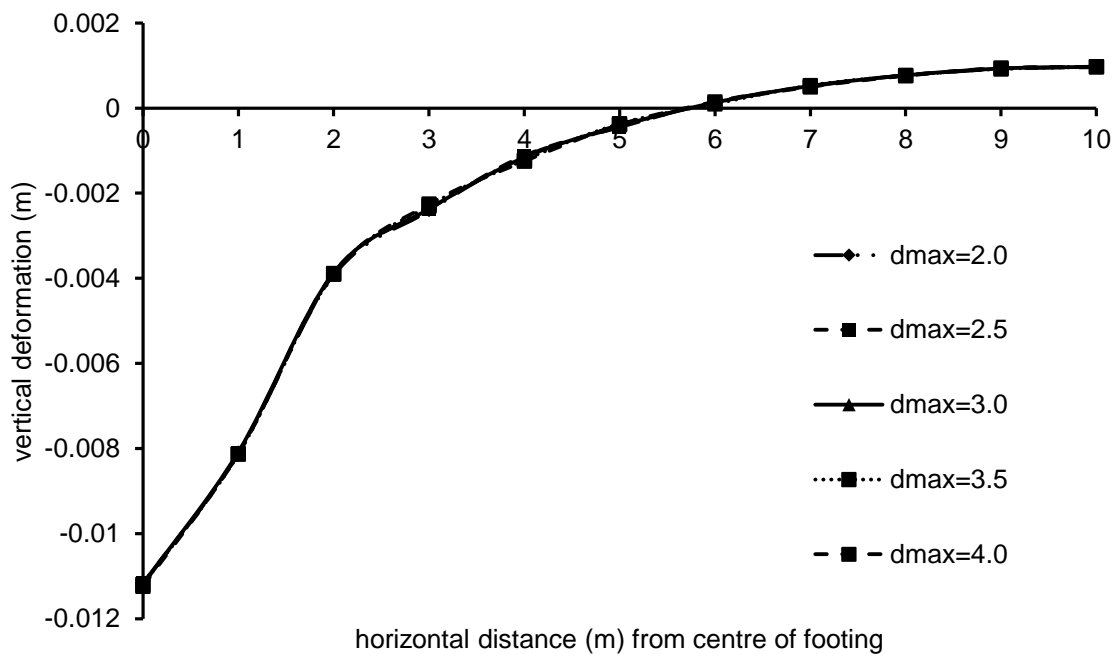


Fig. 15 Variation of vertical deformation on the top surface with distance from centre of footing, for different values of scaling parameter (d_{max})

7. Conclusions

From the study following conclusions can be drawn:

- 1) Vertical deformation decreases with increase in depth and also with increase in horizontal distance from centre of footing whereas horizontal deformation increases initially with increase in horizontal distance and then decreases but decreases with depth continuously.
- 2) Like deformations, stresses also decrease with increase in depth and with increase in horizontal distance from centre of footing.
- 3) With increase in modulus of deformation (E), deformations keep on decreasing. The decrease in deformation is less for higher values of E .
- 4) Modulus of deformation (E) does not have an influence on stress distribution.
- 5) Higher is the Poisson ratio, smaller is the vertical deformation and higher is the horizontal deformation.
- 6) Poisson ratio has a small effect on the stress distribution. At depths close to the surface higher is the Poisson ratio, higher will be the stress and as depth increases there is practically no effect.
- 7) Scaling parameter (d_{\max}) does not have a significant influence on stress distribution. However for depths close to the surface, smaller the value of d_{\max} smaller are the stresses whereas on the surface results are vice versa.

References

- Belytschko, T., Krongauz, Y., Organ, D. and Liu, W.K. (1996), "Smoothing and accelerated computations in the element free Galerkin method", *J. Comput. Appl. Math.*, **74**, 111-126.
- Belytschko, T., Lu, Y.Y. and Gu, L. (1994), "Element free Galerkin methods", *Int. J. Numer. Meth. Eng.*, **37**, 229-256.
- Belytschko, T., Lu, Y.Y. and Gu, L. (1995), "Crack propagation by element free Galerkin methods", *Eng. Fract. Mech.*, **51**(2), 295-315.
- Brighenti, R. (2005), "Application of the element-free Galerkin meshless method to 3-D fracture mechanics problems", *Eng. Fract. Mech.*, **72**, 2808-2820.
- Das, B.M. (2008), *Advanced Soil Mechanics*, Taylor and Francis, London and New York, UK and USA.
- Dolbow, J. and Belytschko, T. (1998), "An introduction to programming the meshless element free galerkin method", *Arch. Comput. Method. E.*, **5**, 207-241.
- Kumar, R.P. and Dodagoudar, G.R. (2009), "Element free galerkin method for two dimensional contaminant transport modelling through saturated porous media", *Int. J. Geotech. Eng.*, **3**(4), 11-20.
- Kumar, R.P. and Dodagoudar, G.R. (2010), "Modelling of contaminant transport through landfill liners using EFGM", *Int. J. Numer. Anal. Method. Geomech.*, **34**, 661-688
- Liu, G.R. and Gu, Y.T. (2005), *An Introduction to Meshfree Methods and Their Programming*, Springer
- Mategaonkar, M. and Eldho, T.I. (2011), "Simulation of groundwater flow in unconfined aquifer using meshfree point collocation method", *Eng. Anal. Bound. Elem.*, **35**(4), 700-707.
- Mategaonkar, M. and Eldho, T.I. (2012), "Two dimensional contaminant transport modeling using meshfree point collocation method (PCM)", *Eng. Anal. Bound Elem.*, **36**(4), 551-561.
- Pandey, S.S., Kasundra, P.K. and Daxini, S.D. (2013), "Introduction of meshfree methods and implementation of element free galerkin (efg) method to beam problem", *Int. J. Theor. Appl. Res. Mech. Eng.*, **2**(3), 2319-3182.
- Park, Y.C. and Leap, D.I. (2000), "Modelling groundwater flow by the element-free Galerkin (EFG) method", *Geosci. J.*, **4**(3), 231-241.

- Poulos, H.G. and Davis, E.H. (1974), *Elastic Solutions for Soil and Rock Mechanics*, John Wiley and Sons, Inc., New York, USA.
- Ranjan, G. and Rao, A.S.R. (2011), *Basic and Applied Soil Mechanics*, New Age International, New Delhi, India.
- Thomas, A., Eldho, T.I. and Rastogi, A.K. (2013), "A comparative study of point collocation based meshfree and finite element methods for groundwater flow simulation", *ISH J. Hyd. Engg*, **20**(1), 65-74.
- Wang, Z.L. and Li, Y.C. (2006), "Analysis of factors influencing the solution of the consolidation problem by using an element-free Galerkin method", *Comput. Geosci.*, **32**, 624-631.